Fluorescence Anisotropy Imaging Microscopy Maps Calmodulin Binding during Cellular Contraction and Locomotion

Albert H. Gough and D. Lansing Taylor

Center for Light Microscope Imaging and Biotechnology, and Department of Biological Sciences, Carnegie Mellon University, Pittsburgh, Pennsylvania 15213

Abstract. Calmodulin is a calcium transducer that activates key regulatory and structural proteins through calcium-induced binding to the target proteins. A fluorescent analog of calmodulin in conjunction with ratio imaging, relative to a volume indicator, has demonstrated that calmodulin is uniformly distributed in serum-deprived fibroblasts and there is no immediate change in the distribution upon stimulation with complete serum. The same fluorescent analog of calmodulin together with steady state fluorescence anisotropy imaging microscopy has been used to define the temporal and spatial changes in calmodulin binding to cellular targets during stimulation of serum-deprived fibroblasts and in polarized fibroblasts during wound healing. In serum-deprived fibroblasts, which exhibit a low free calcium ion concentration, a majority of the fluorescent analog of calmodulin remained unbound (fraction bound, $f_B < 10\%$). However, upon stimulation of the serum-deprived cells with complete serum, calmodulin binding (maximum $f_B \approx 95\%$) was directly correlated with the time course of the elevation and decline of the free calcium ion concentration, while the contraction of stress fibers continued for an hour or more. Calmodulin binding was also elevated in the leading lamellae of fibroblasts (maximum $f_B \approx 50\%$) during the lamellar contraction phase of wound healing and was spatially correlated with the contraction of transverse fibers containing myosin II. Highly polarized and motile fibroblasts exhibited the highest anisotropy (calmodulin binding) in the retracting tails and in association with contracting transverse fibers in the cortex of the cell. These results suggest that local activation of myosin II–based contractions involves the local binding of calmodulin to target proteins. The results also demonstrate a powerful yet simple mode of light microscopy that will be valuable for mapping molecular binding of suitably labeled macromolecules in living cells.

UNDERSTANDING the chemical and molecular basis of cell functions requires the definition of the temporal and spatial interplay of ions, metabolites, macromolecules, and organelles in living cells (Taylor and Wang, 1980; Taylor et al., 1984; Kolega and Taylor, 1991; Taylor et al., 1992). Calcium, in particular, is a second messenger which has a number of intracellular effects, some of which are mediated by calmodulin. In vitro biochemical data suggest that the calcium–calmodulin complex leads to a modification in the phosphorylation state of key regulatory proteins by binding to and activating protein kinases and phosphatases, as well as cyclic nucleotide phosphodiesterases (Cohen and Klee, 1988). In the specific case of nonmuscle and smooth muscle contractile events, studies of myosin II regulation suggest the following sequence of events: stimulation → a rise in free calcium concentration ($[Ca^{2+}]_f$)[1] → calcium binding to calmodulin → the calcium–calmodulin complex binding to and activating myosin II light chain kinase (MLCK)[1] and other targets → MLCK phosphorylation of the 20-kD regulatory light chain of myosin II (LC_{20}) → permitting the interaction of myosin II with actin to produce a contractile force (Sellers and Adelstein, 1987). A key step in the calmodulin-based signaling sequence involves the binding of the calcium–calmodulin complex to MLCK and other calmodulin targets upon the elevation of $[Ca^{2+}]_f$.

Physiological indicators and fluorescent analogs of specific proteins have established a temporal–spatial relationship between calcium ion fluctuations, calcium binding to calmodulin, and the contraction of stress fibers containing actin and myosin II. Indicators of $[Ca^{2+}]_f$ demonstrate that $[Ca^{2+}]_f$ is very low in serum-deprived cells ($\leqslant 10^{-7}$ M) and that when stimulated with serum or specific growth factors the $[Ca^{2+}]_f$ transiently increases to near 10^{-6} M (McNeil et al., 1985; McNeil and Taylor, 1987; Byron and Villereal, 1989; Tucker and Fay, 1990; Hahn et al., 1992). Stress fibers in serum-deprived cells exhibit a semi-sarcomeric organization of fluorescent analogs of myosin II, and can be shown

1. *Abbreviations used in this paper*: ATR, acetamidotetramethylrhodamine; CaM, calmodulin; CS, calf serum; EBS, Earles Balanced Salts; FAIM, fluorescence anisotropy imaging microscopy; MLCK, myosin II light chain kinase; PDE, 3′-5′ cyclic nucleotide phosphodiesterae; SSFA, steady state fluorescence anisotropy.

to contract following stimulation (Giuliano and Taylor, 1990; Kolega et al., 1991; Giuliano et al., 1992). Temporally, the calcium transient and the resulting contraction are not tightly coupled, since the calcium response lasts only a few minutes, while the contraction continues for about an hour (Giuliano and Taylor, 1990; Hahn et al., 1992).

Using a new fluorescent analog of calmodulin, MeroCam 1, as an optical biosensor (Hahn et al., 1990), it has been shown that calmodulin binds calcium in phase with the elevation and decline of $[Ca^{2+}]_f$ (Hahn et al., 1992). It has also been shown that patterns of elevated $[Ca^{2+}]_f$ and calcium binding to calmodulin (Hahn et al., 1992) colocalize with contracting transverse fibers in fibroblasts undergoing the lamellar contraction phase of wound healing (DeBiasio et al., 1988). Examination of the phosphorylation state of the LC_{20} by biochemical assays reveals that there is a sustained increase in phosphorylation following serum stimulation that continues through the ~1-h contraction time (Giuliano et al., 1992). This implies either that the MLCK remains activated despite the transience of the increase in $[Ca^{2+}]_f$ and calcium binding to calmodulin or that the phosphatase which dephosphorylates the LC_{20} remains inactivated. In this study we have mapped calmodulin binding relative to contracting fibers containing a fluorescent analog of myosin II, to explore the suggested role of calmodulin in regulating this contraction.

Interactions of calmodulin with MLCK and other targets in living cells are predicted to result in a substantial decrease in the mobility of calmodulin since calmodulin is a relatively small protein (M_r = 16,790). Indeed, Luby-Phelps et al. (1985) and Stemple et al. (1988), using FRAP to measure the translational mobility of fluorescent analogs of calmodulin in living cells provide evidence that supports this prediction. In interphase Swiss 3T3 cells, an immobile fraction of 15–20% of the fluorescent calmodulin was present in all cells, while some cells exhibited calmodulin localization to stress fibers and in other cells the calmodulin was diffusely distributed (Luby-Phelps et al., 1985). In mitotic PtK1 cells, it was shown that calmodulin associates with the spindle poles, probably through an interaction with microtubule associated proteins, since no direct interaction with microtubules has been observed (Stemple et al., 1988). These results and others (Cohen and Klee, 1988) suggest that calmodulin activation in vivo may be more complicated than the simple $[Ca^{2+}]_f$-dependent interaction observed using in vitro systems of a few purified components. However, the dependence of the translational mobility, as measured by FRAP, on the structural organization of the cytoplasmic matrix, as well as the hydrodynamic properties of the molecule and the solution viscosity, complicates the interpretation of translational mobility measurements specifically in terms of binding interactions (Luby-Phelps et al., 1987; Luby-Phelps et al., 1988; Kao et al., 1993). The rotational mobility, however, is predicted to be a much more sensitive indicator of binding interactions (see Appendix) and is relatively insensitive to the long range organization of the cytoskeletal meshwork (Fushimi and Verkman, 1991; Kao et al., 1993). Measurements of rotational mobility by steady state fluorescence anisotropy imaging microscopy (FAIM) also allow higher spatial and temporal resolution than FRAP, facilitating the correlation of changes in rotational mobility, and therefore binding, with the distributions of other cellular components such as myosin II and other physiological parameters such as $[Ca^{2+}]_f$. Finally, FAIM is a relatively simple mode of light microscopy that can be easily added to an existing imaging system.

We address five questions in this paper. First, what is the distribution of calmodulin in serum-deprived cells and is there a change following stimulation with serum? Second, is calmodulin freely mobile in serum-deprived cells at low $[Ca^{2+}]_f$ as predicted by in vitro biochemistry? Third, does calmodulin bind to intracellular targets in response to calcium signaling? Fourth, does the release of calmodulin from the targets follow the kinetics of the decay of the calcium transient? Fifth, are there correlations between the distribution of myosin II in contracting fibers and calmodulin binding as would be predicted from the solution biochemistry?

Materials and Methods

Materials

DTT, EGTA, MOPS, Pipes, FITC- and TRITC-calmodulin (CaM) spinach calmodulin, Sephadex G-25, Earles Balanced Salts (EBS), and amino acid mixture were purchased from Sigma Immunochemicals (St. Louis, MO); calmodulin-free 3′-5′ cyclic nucleotide phosphodiesterase (PDE), calmodulin-free alkaline phosphatase, and calmodulin-free adenosine deaminase were obtained from Boehringer-Mannheim Biochemicals (Indianapolis, IN); tetramethylrhodamine and fluorescein isothiocyanate-labeled 10-kD dextrans and monobromobimane were obtained from Molecular Probes, Inc. (Junction City, OR); and all other chemicals were reagent grade.

Preparation of Fluorescent Analogs

Calmodulin activity assays and binding assays were performed in an assay buffer consisting of 100 mM MOPS, pH 7.0, 60 mM KCl, 2 mM $MgCl_2$, 2.5 mM EGTA, and varying amounts of 0.1 M $CaCl_2$ standard solution (Orion Research Inc., Cambridge, MA) to yield the indicated $[Ca^{2+}]_f$. Samples for microinjection were prepared in injection buffer consisting of 2 mM Pipes, pH 7.0. Bovine brain calmodulin, prepared and characterized as previously described (Hahn et al., 1990) was used as a standard for protein and activity assays.

Spinach calmodulin was used to make the monobromobimane analog of calmodulin (Bimane-CaM) because it contains a single cysteine and labeling at this site appears to have little or no effect on its biological activity (Mills et al., 1988). The lyophilized spinach calmodulin was dissolved in 10 mM MOPS (pH 7.0), 2 mM EGTA and 0.5 mM DTT, at a concentration of 5 mg/ml. After the reduction, the DTT was removed by passing the solution through a Sephadex G-25 column (1 × 10 cm) equilibrated with the same buffer without DTT and selecting the fractions with maximum absorbance at 280 nm. Bimane-CaM was prepared by the addition of a fivefold molar excess of 1 mM monobromobimane in ethanol to the ~2 mg/ml solution of spinach calmodulin. The mixture was stirred for 2 h at room temperature, and then exhaustively dialyzed against distilled water. The labeled calmodulin (dye/protein ~1.0) was either lyophilized or frozen and stored at −60°C.

The lyophilized powders of FITC-CaM (dye/protein = 0.8) and TRITC-CaM (dye/protein = 0.8) were resuspended in 50 mM MOPS, pH 7.2, and dialyzed against assay buffer or injection buffer before use. FITC-CaM was microinjected at a concentration of ~4 mg/ml in injection buffer.

Acetamidotetramethylrhodamine-myosin II (ATR-myosin II) was prepared as described previously (DeBiasio et al., 1988). The ATR-myosin II had a dye to protein ratio of ~4.8 and was prepared for microinjection at a concentration of ~4 mg/ml in a buffer consisting of 2 mM Pipes, pH 7.0 (25°C), 0.1 mM ATP, 0.1 mM DTT, 0.05 mM $MgCl_2$.

Characterization of Fluorescent Analogs

The activation of PDE by calmodulin in assay buffer was measured by a coupled enzyme assay (Schiefer, 1986). A computer program (adapted from Robertson and Potter, 1984) was used to calculate the amount of 0.1 M $CaCl_2$ standard solution to add to give the desired $[Ca^{2+}]_f$. For steady state fluorescence anisotropy (SSFA) measurements, a calmodulin concentration of 1 μM and an ionic strength of ~100 mM were used to simulate physiolog-

ical conditions. PDE activity assays were used to determine the concentration of PDE mixture which nearly saturated the calmodulin by titrating 10 ng/ml of calmodulin with the PDE mixture to saturation, fitting a binding curve by nonlinear least squares, and taking the concentration where activity was 95% maximal. This concentration was then scaled up equivalently to the calmodulin concentration (final concentration of PDE mixture was 0.5 mg/ml). Measurements were made in a 24°C temperature controlled and stirred 1 cm cuvette.

Tetramethylrhodamine-labeled neutral dextrans were used as a volume marker in ratio imaging studies which map the relative distribution of total calmodulin (DeBiasio et al., 1988). The lyophilized powder was dissolved in injection buffer at 10 mg/ml stock concentration. The stock was diluted approximately fivefold by mixing with 8 mg/ml FITC-CaM stock and injection buffer, giving final injection concentrations of ~2 mg/ml-labeled dextran and ~4 mg/ml FITC-CaM.

Cell Culture and Preparation

For serum stimulation, cells were prepared as described previously (Giuliano and Taylor, 1990) except as follows. About 12 h before stimulation, the 0.2% serum medium was changed to a medium consisting of bicarbonate buffered EBS, amino acid mixture, and 0.2% calf serum (CS). The EBS medium was used to avoid the high background signal in the fluorescein channel produced by riboflavin fluorescence in complete media. Cells were microinjected with a 4 mg/ml stock solution of FITC-CaM in injection buffer, 1–3 h before stimulation as previously described (Luby-Phelps et al., 1985). Coverslips were mounted in a modified Sykes-Moore chamber fitted with perfusion ports (Bright et al., 1987). Cells were stimulated on the temperature controlled microscope stage by perfusion with EBS containing 10% CS.

Cells were prepared for would healing experiments as previously described (DeBiasio et al., 1988). Briefly, cells were plated as above and grown to confluence. About 24 h after reaching confluence, cells were wounded by scraping a region with a razor blade in order to produce two clean wound edges. Cells along the edge of the wound were coinjected with ATR-myosin II (1.6 mg/ml) and FITC-calmodulin (2 mg/ml) approximately 3–5 h after wounding. The coverslips were mounted in a Sykes-Moore chamber 1–3 h postinjection. Because perfusion was unnecessary, coverslips were mounted without the perfusion ring forming a 0.25-mm thick sealed chamber. This thin chamber reduced the background riboflavin fluorescence enough to allow the use of complete media in wound healing studies.

Fluorescence Spectroscopy

All fluorometer measurements were made on a Fluorolog-2 (SPEX, Metuchen, NJ) equipped with 450 W xenon arc lamp, dual grating monochromators and Glan-Thompson polarizers. SSFA measurements of Bimane-CaM, FITC-CaM, and TRITC-CaM were made with excitation at 380, 495, and 556 nm and emission at 470, 520, and 580 nm, respectively. For FITC- and TRITC-CaM the excitation and emission bandwidths were 2 and 4 nm, respectively. For Bimane-CaM the excitation and emission bandwidths were 4 and 10 nm, respectively, because Bimane-CaM has a weaker absorbance and the xenon lamp output is lower at the shorter excitation wavelength.

Fluorescence Microscopy

Images were acquired on a prototype Zeiss microscope (Carl Zeiss, Oberkochen, Germany) using a 75 W xenon arc lamp, a thermoelectrically cooled CCD camera (CH220; Photometrics LTD, Tucson, AZ) containing a Thompson 576 × 384 CCD with 14-bit precision and a Zeiss Plan Neofluor 40× (1.3 NA) objective lens. Bimane-CaM was imaged with Zeiss BP 356/60 excitation and Omega (Brattleboro, VT) 470 DF 40-emission filters. FITC-CaM was imaged with Zeiss BP 484/20 excitation and BP 546/50 emission filters. ATR-myosin II was imaged with Omega 530 DF 30 excitation and 580 DF 30 emission filters. A mounted film polarizer (Melles Griot, Irvine, CA), with orientation fixed to give horizontally polarized light, was inserted in the epifluorescence path. A standard Zeiss rotatable analyzer was inserted in the emission path and aligned perpendicular to the excitation polarizer by minimizing the intensity of the reflection from a front surface mirror. The analyzer was then rotated 90° for the parallel orientation.

For the serum stimulation experiments images were integrated for 3 s with a 0.3 OD neutral density filter in the excitation path and binned 2 × 2 on the CCD to increase the signal to noise ratio. Images were acquired the same for wound healing studies except without binning, to obtain better spatial resolution.

Ratio images of FITC-CaM to tetramethylrhodamine–dextran were obtained using the Multimode Light Microscope Workstation (Biological Detection Systems, Inc., Pittsburgh, PA). The methods were the same as developed previously for determining the relative distribution of fluorescent analogs (DeBiasio et al., 1988; Pagliaro and Taylor, 1988).

Demonstration of the Ability to Image Fluorescence Anisotropies

To test the accuracy of the FAIM measurements, solutions of sodium fluorescein in glycerol were prepared and fluorescence anisotropies were measured both by conventional fluorometry and by steady state FAIM. Fig. 1 compares these measurements and shows that at low magnification and low numerical aperture the values obtained by the two methods are the same, within the error of the measurements. At high magnification and high numerical aperture (40× 1.3 NA), the values obtained by imaging are consistently 87% of the fluorometer measures, as determined by linear least squares analysis (see Fig. 1, legend). This result demonstrates that although the anisotropy values are somewhat reduced in the imaging measurements, they are strongly correlated with the fluorometer measures and therefore can simply be corrected to true sample anisotropies.

Selection of a Fluorescent Analog for FAIM

To find a fluorescent analog with both sensitivity to changes in rotational correlation time and adequate brightness (defined as the product of the extinction coefficient and the quantum yield of fluorescence) (see Taylor et al., 1986; Waggoner, 1990) for intracellular imaging, we screened three fluorescent analogs of calmodulin; TRITC-CaM, FITC-CaM and Bimane-CaM (see Table I). The viscosity of cytoplasm, as measured by time resolved fluorescence anisotropy, has been reported to be in the range of 1.2–1.4 cP

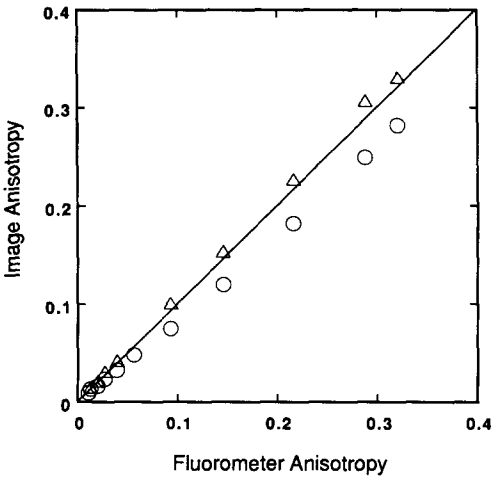

Figure 1. Anisotropy of fluorescein in glycerol solutions measured by steady state FAIM and in a standard fluorometer. Solutions of 3 μM sodium fluorescein buffered with 10 mM MOPS (pH 7.0) were loaded into 200-μm path length flat capillaries for imaging or 1 cm cuvettes for fluorometer measures. Samples contained glycerol in fractions varying from 0 to 99% wt/vol. The effect of numerical aperture (NA) on imaging anisotropies was investigated by using two different objectives, a Zeiss 5×, 0.15 NA (Δ) and a Zeiss 40×, 1.3 NA (○). The G correction factor (described in the Appendix) was determined separately for each objective. The line shown has a slope of 1 and therefore represents identity of the measurements by the two methods. A line fit by linear least squares to the data points obtained at 40× has a slope of 0.87, and intercept of 0.002, and a correlation coefficient of 0.999 (line not shown). The deviation to somewhat lower anisotropies for the images acquired at 40×, 1.3 NA, most likely results from depolarization at high NA (Axelrod, 1989).

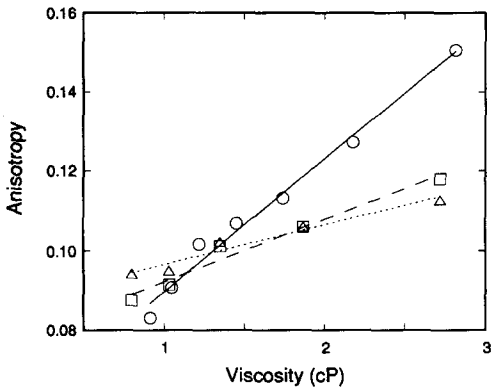

Figure 2. Viscosity dependence of the SSFA for three fluorescent analogs of calmodulin. SSFA was measured in the fluorometer on 1 μM solutions of Bimane-CaM (○, ——), FITC-CaM (□, – – –), and TRITC-CaM (△, ·····) in assay buffer as described in Materials and Methods. The viscosity (at 24°C) was increased by the addition of increasing fractions (wt/vol) of glycerol. The standard deviations of the data points were about the size of the markers. The slopes of the lines fit by linear regression indicate the relative response, of each of the analogs, to the increased rotational correlation time resulting from increased viscosity.

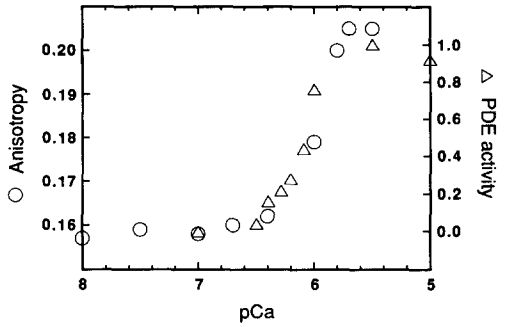

Figure 3. Calcium dependence of the interaction between FITC-CaM and PDE determined by enzyme assay (Δ) and SSFA (○). The anisotropy of 1 μM solutions of FITC-CaM in assay buffer, in the presence of nearly saturating amounts of PDE, were measured in the fluorometer. The solution, in a stirred and temperature-controlled (24°C) cuvette, was titrated with calcium standard solution and the anisotropy measured at the indicated $[Ca^{2+}]_f$ concentrations. The normalized PDE activity at similar $[Ca^{2+}]_f$ was measured on a separate set of samples by a coupled enzyme assay (Schiefer, 1986).

(Fushimi and Verkman, 1991). When we measured the change in SSFA for each of the analogs, as a function of viscosity from 1 to 3 cP (Fig. 2), Bimane-CaM exhibited the greatest increase in anisotropy (~90%), as expected because of its theoretically optimal lifetime (see Appendix), while FITC-CaM increased ~40%, and TRITC-CaM ~30%. Because Bimane-CaM was most sensitive to the change in viscosity (as indicated by the large slope in Fig. 2) and therefore rotational correlation time, we used Bimane-CaM for our initial imaging experiments. In the PDE assay, Bimane-CaM had nearly the same activity as unlabeled bovine brain calmodulin (data not shown).

We microinjected serum-deprived Swiss 3T3 cells with Bimane-CaM in injection buffer. Although the perinuclear region was just bright enough to be seen by eye, long integration times (≥10 s) were required to record any detail in the periphery of the cell (data not shown). Because the addition of the two polarizers required for FAIM measurements reduces the fluorescence signal to ~25%, and since the anisotropy (Appendix, Eq. A1) involves taking the difference between two images, the signal to noise ratio in the calculated Bimane-CaM FAIM images was too low to be of practical value. FITC-CAM is ~15-fold brighter than Bimane-CaM (Table I), however, and more sensitive to anisotropy differences than TRITC-CaM (Fig. 2). We therefore chose to test FITC-CaM as an intracellular probe of calmodulin binding.

SSFA of FITC-CaM Can Be Used to Detect the Binding of Calmodulin to Target Proteins

To test the biological activity of FITC-CaM we measured the calcium dependence of the activation of PDE and the maximal level of activation of PDE using a coupled enzyme assay. The calcium dependence of the activation of PDE (Fig. 3) showed a transition at ~10^{-6} M $[Ca^{2+}]_f$, indistinguishable from unlabeled calmodulin and consistent with the calcium dependence of the interaction of calmodulin with other target proteins (Cohen and Klee, 1988). In the presence of saturating $[Ca^{2+}]_f$ (1 mM), FITC-CaM–activated PDE to the same extent as unlabeled bovine brain calmodulin (data not shown).

Table I. Spectral Properties of Derivatives of the Three Fluorophores Used to Label Calmodulin

Fluorophore	ε (×10^{-3}) ($M^{-1}cm^{-1}$)	Φ_F*	λexc (nm)	τ_f (ns)
Bimane‡	5.3	0.26§	380	9.5‖
FITC**	60	0.23	490	4.0
TRITC‡‡	85	0.28	554	2.0

* Quantum yield of fluorescence.
‡ Monobromobimane derivative of BSA (Chen and Scott, 1985).
§ Kosower and Kosower (1987).
‖ All fluorescence lifetimes are taken from Chen and Scott (1985).
** Taylor et al. (1986).
‡‡ Waggoner (1990).

The intracellular SSFA of a calmodulin analog will depend both on the cytoplasmic viscosity and the effective size of calmodulin, either free or bound to a target protein. To test the sensitivity of FITC-CaM to changes in rotational mobility resulting from calcium-dependent interactions with other proteins, we measured the anisotropy of a mixture of 1 μM FITC-CaM in the presence of near saturating amounts of PDE as a function of $[Ca^{2+}]_f$ (Fig. 3). These data indicate that at least a 32% increase in anisotropy occurs as a result of FITC-CaM binding to PDE in aqueous solution. Fig. 3 also slows that the half maximal binding as measured by anisotropy and the half maximal PDE activation as measured by a coupled enzyme assay both occur at the same $[Ca^{2+}]_f$, ~10^{-6} M.

The fraction of calmodulin bound to targets (f_B) can be determined from SSFA measurements using the equation (Lakowicz, 1983):

$$f_B = (r - r_F)/(r_B - r_F), \quad (1)$$

where r is the SSFA, r_F is the SSFA of the free molecule, and r_B is the SSFA of the bound molecule. Fluorescence anisotropy imaging measurements of dye molecules indicate that the intracellular viscosity is only slightly greater than that of water and that it is relatively insensitive to a variety of cellular perturbations (Fushimi and Verkman, 1991; also see Discussion). The SSFA of free intracellular FITC-CaM is therefore estimated to be the same as that of the molecule in water. We measured the SSFA of FITC-CaM in water and found that r_F = 0.088. Because the SSFA is strongly dependent on molecular size (see Appendix) the SSFA of bound FITC-CAM can be estimated from the SSFA of FITC-CaM in the presence of a nearly saturating amount of PDE and 1 mM $[Ca^{2+}]_f$, giving r_B = 0.205 (Fig. 3). Any difference in the intracellular viscosity will primarily affect our estimate of r_F, since bound calmodulin is essentially immobilized and therefore not much effected by viscosity. Our estimate of f_B when f_B is near 0 then, can be considered as an upper limit, since the intracellular viscosity may be somewhat greater than that of water. We will however, only use the f_B as a relative indicator of the state of calmodulin binding.

Results

FITC–Calmodulin Is Freely Mobile in Serum-deprived Cells

FITC-CaM was microinjected into serum-deprived Swiss

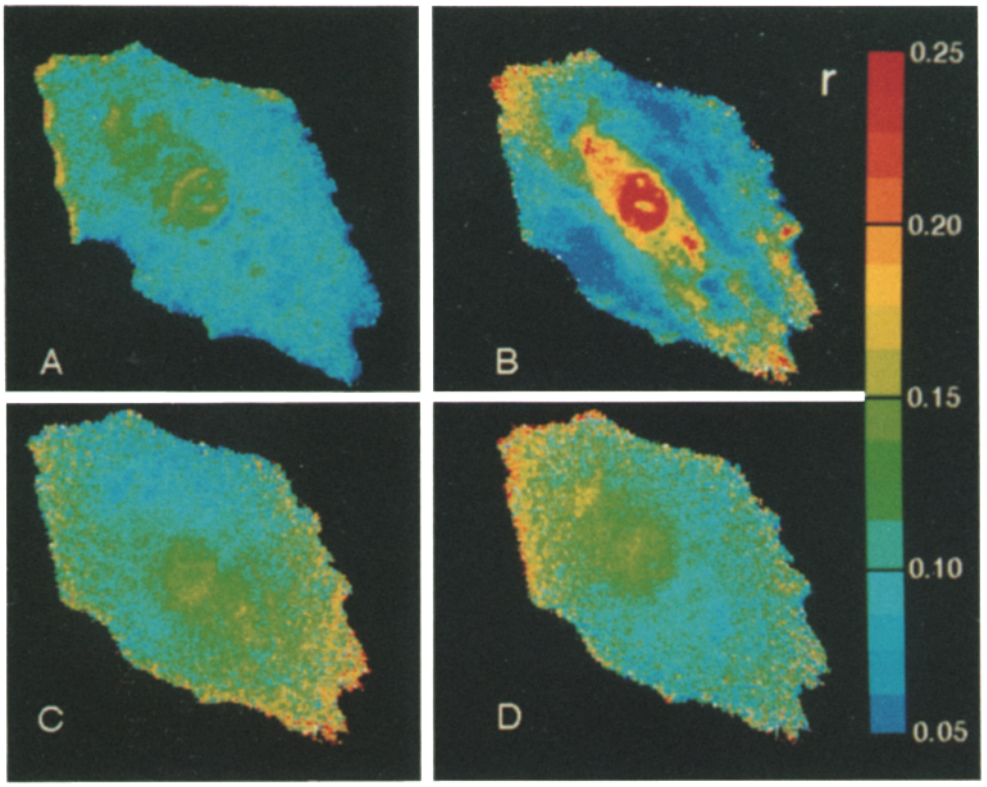

Figure 4. Steady state FAIM images of serum-deprived cells stimulated with media containing 10% CS. The cells were plated in DME + 10% CS which was replaced with DME + 0.2% CS 48 h before stimulation. Cells were injected with 4 mg/ml FITC-CaM and allowed to recover for ≈1 h. The coverslip was mounted in a temperature-controlled chamber for observation on the microscope. Image pairs were acquired before stimulation and at approximately 30-s intervals post-stimulation. SSFA before stimulation (*a*), 60 s (*b*), 90 s (*c*), and 120 s (*d*) after stimulation with media containing 10% CS. The color bar indicates the anisotropy scale from 0.05 (*blue*) to 0.25 (*red*). The SSFA was consistently higher in the nucleus of serum deprived cells (*a*) which could be either a viscosity effect or an indication of increased bound fraction. Bar, 10 μm.

3T3 cells, a prestimulation image pair was acquired, the cells were perfused with medium containing 10% CS and a sequence of image pairs were acquired at 30-s intervals (Fig. 4). Fig. 4 *a* is a prestimulation FAIM image of FITC-CaM in a serum-deprived cell. The anisotropy was very uniform and had an average value of 0.10 (±0.02) in 20 cells investigated, comparable to that of FITC-CaM in water (0.088). This anisotropy value is consistent with a very low bound fraction of calmodulin ($f_B \leq 10\%$) at low $[Ca^{2+}]_f$ and an intracellular microviscosity not much higher than that of water (1.0 cP). This low viscosity is supported by time-resolved fluorescence anisotropy measurements of dye molecules in cells which yielded a uniform local viscosity of 1.2–1.4 cP (Fushimi and Verkman, 1991). Our results demonstrate that the cytoplasmic viscosity seen by a small tumbling protein, like that of a free dye, primarily reflects the viscosity of the water solvent. Furthermore, while measurements by FRAP indicate that for most proteins, including calmodulin, the translational mobility in cells is reduced about an order of magnitude from that in water (Luby-Phelps et al., 1987), the rotational mobility of FITC-CaM in cells at low $[Ca^{2+}]_f$ more nearly reflects its mobility in water.

Calmodulin Binding Follows the Time Course of Calcium Elevation and Decline

Fig. 4 (*b–d*) are FAIM images of the same cell at time points following stimulation with medium containing 10% CS. The anisotropy increased rapidly (Fig. 4 *b*) and diminished nearly as rapidly, consistent with the time course of the calcium response in these cells (McNeil et al., 1985; McNeil and Taylor, 1987; Byron and Villereal, 1989; Tucker and Fay, 1990; Hahn et al., 1992). There was heterogeneity in the response (Bright et al., 1989*b*) but the kinetics of the rise and fall of the transient calmodulin binding were consistent among the cells in which a response was recorded. Fig. 5 *a* is a plot of the average of the histograms of anisotropy values

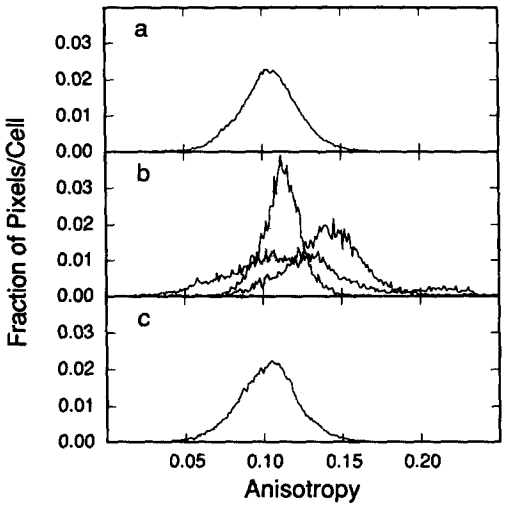

Figure 5. Plot of the distributions of anisotropy values in cells before, immediately after and several minutes after stimulation. The histograms of the SSFA values in individual cells were normalized to an area of 1, and averaged. The prestimulation histograms (*a*) have a mean SSFA of 0.10 (SDEV = 0.02, n = 20). The spatial and intercellular heterogeneity of the response is illustrated by the histograms of the SSFA in individual cells immediately after stimulation with 10% CS (*b*) and Fig. 4 *b*. Within 10 min after stimulation the distribution of SSFA values (*c*) is similar to prestimulation (mean SSFA of 0.10, SDEV = 0.02, n = 10).

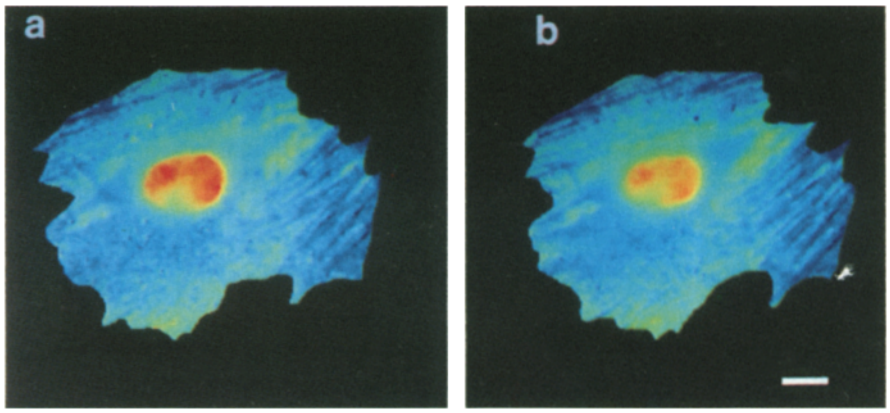

Figure 6. Fluorescence ratio images depict the FITC-CaM distribution in serum deprived cells stimulated with 10% CS. Cells were prepared as described in Fig. 4 and were coinjected with 4 mg/ml FITC-CaM and 2 mg/ml tetramethylrhodamine–dextran (10 kD), a volume marker. (*a*) Distribution before stimulation and (*b*) distribution 3-min poststimulation. The pseudocolored images show relatively high ratios, and therefore FITC-CaM concentrations, as red and low ratios as blue. Image ratios were taken from before stimulation to more than 30-min poststimulation with no measurable change. The concentration of FITC-CaM relative to dextran in the cytoplasm was essentially uniform and constant over time, independent of serum stimulation. The concentration of FITC-CaM in the nucleus was consistently higher than in the cytoplasm. Bar, 10 μm.

in prestimulation cells (mean = 0.10, sdev = 0.02). Fig. 5 *b* illustrates the shift in the distribution of anisotropy values within a representative set of individual cells. Fig. 5 *c* shows the average of the histograms of cells 4 to 15 min after stimulation with 10% CS (mean = 0.10, sdev = 0.02). These results demonstrate that the contraction of myosin II–based stress fibers, which follows stimulation and continues for an hour or longer (Giuliano and Taylor, 1990), does not require a continuous binding of a large fraction of calmodulin to target proteins in order to function.

The anisotropy of FITC-CaM in the nucleus of serum deprived Swiss 3T3 cells was consistently about 20% higher

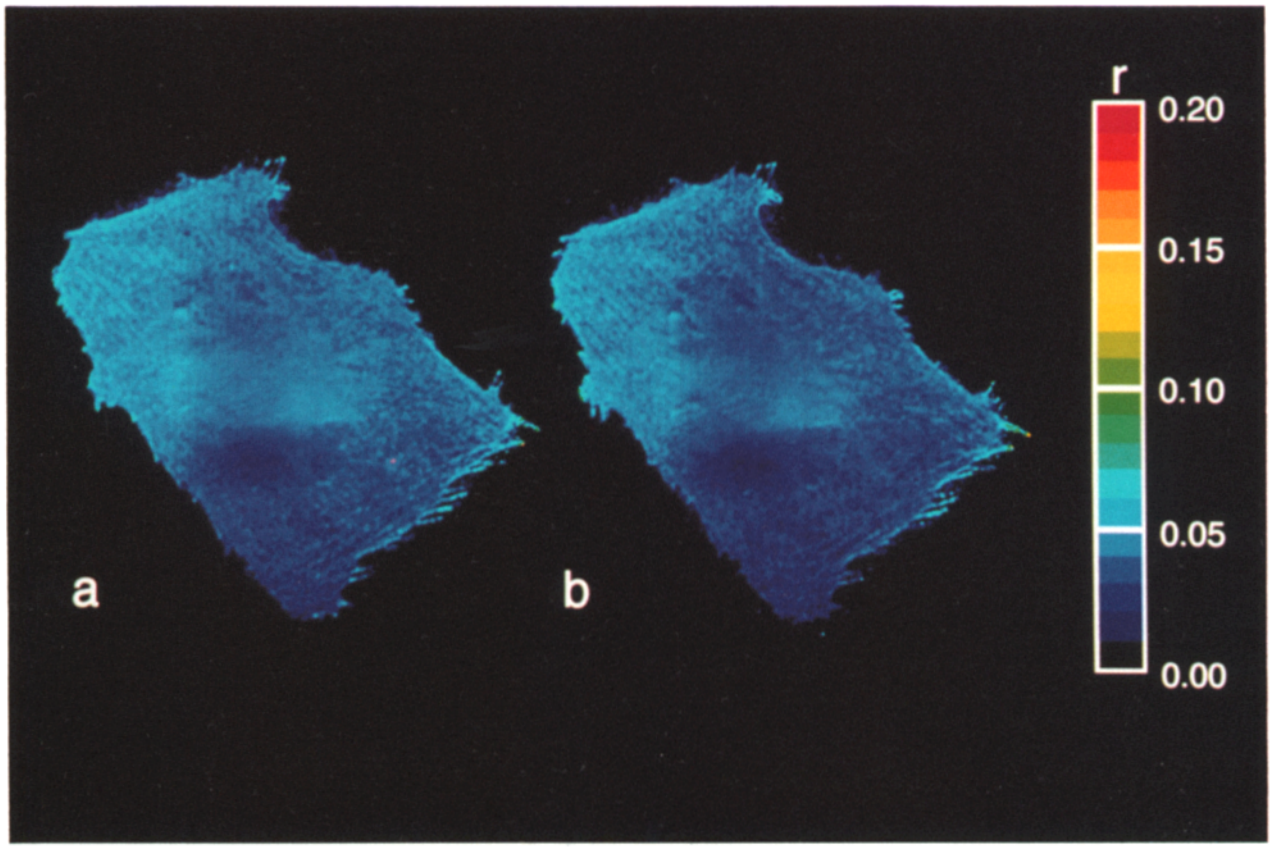

Figure 7. FAIM images of fluorescein dextran in serum-stimulated cells. Cells were prepared as in Fig. 4 and a 5 mg/ml solution of FITC-dextran (10 kD) in injection buffer was microinjected. Images were recorded (*a*) before stimulation, (*b*) immediately following stimulation. The anisotropy was very uniform over the cell, including the nucleus, and the mean anisotropy was comparable to that of the same dextran in water ($r = 0.030$). Images were recorded for up to 2 h poststimulation. There was no evidence of a change in the SSFA of FITC–dextran after stimulation. The anisotropy remained uniform even in cytoplasmic domains exhibiting contraction (Giuliano and Taylor, 1990). The color bar indicates the anisotropy scale from 0.00 (*blue*) to 0.20 (*red*). Bar, 10 μm.

than in the surrounding cytoplasm (Fig. 4 *a*). Furthermore, upon stimulation with serum, the anisotropy in the nucleus increased to about the anisotropy measured in vitro for bound FITC-CaM (Fig. 4 *b*). This increase is consistent with observed changes in calcium concentration in nuclei (Tucker and Fay, 1990; Hahn et al., 1992) and the possible calmodulin regulation of specific gene expression following stimulation of cells (see McNeil and Taylor, 1987).

FITC–Calmodulin Is Uniformly Distributed in Serum-deprived Cells

Although the anisotropy is normalized to the total emission, changes in the SSFA could be attributed to concentration induced quenching or alteration of the brightness of FITC-CaM by interaction with other cellular components. We tested for changes in the brightness of FITC-CaM relative to tetramethylrhodamine–dextran, a volume indicator, by ratio imaging. FITC-CaM and tetramethylrhodamine–dextran were co-injected into serum-deprived Swiss 3T3 cells. Fig. 6 shows a pair of ratio images depicting the relative concentration of calmodulin before and ~4 min after the stimulation of serum-deprived cells. FITC-CaM is relatively uniformly distributed in serum-deprived cells (Fig. 6 *a*), although the nucleus consistently shows an elevated concentration of calmodulin relative to the volume marker. There is little or no change in the distribution of calmodulin immediately following stimulation (Fig. 6 *b*). We examined cells for up to 5 min poststimulation and found no evidence for any change in the local FITC-CaM concentration or brightness in this time frame. Therefore, the change in SSFA measured early in the stimulation response (Fig. 4, *a* and *b* and 5, *a* and *b*) cannot be due to artifacts of fluorescein fluorescence. However, later stages of contraction exhibited some apparent concentration of calmodulin in contracting domains (Hahn et al., 1992).

Changes in Rotational Mobility of FITC–CaM Are Not the Result of Changes in Intracellular Viscosity

To test whether the change in SSFA following serum stimulation reflected an increase in the viscosity of the cytoplasm, FAIM measurements were made on neutral, fluorescein labeled dextrans (10 kD) microinjected into cells. Fig. 7 shows the typical distribution of SSFA observed in cells during stimulation. The average value of the anisotropy in Fig. 7 is 0.033 (± 0.007), comparable to the anisotropy of the same fluorescein dextrans in water (data not shown). The uniformity of the dextran SSFA across the cell was consistent between cells and did not change during contraction, even in regions where condensation of cytoplasmic structures could be observed an hour or more after stimulation.

Calmodulin Binds to Domains in the Leading Lamellae of Migrating Fibroblasts That Exhibits Contraction of Transverse Fibers

We used the wound healing model to generate polarized, motile cells with a well-defined spatial organization of actin and myosin II in transverse fibers (DeBiasio et al., 1988; Fisher et al., 1988; Conrad et al., 1989; Conrad et al., 1993), a predictable sequence of contractile events (DeBiasio et al., 1988), and slow kinetics which allow observation during these contractile events. In the wound healing model, fluorescent analogs of myosin II are incorporated into transverse fibers which form behind the leading edge, the transverse fibers are transported toward the nucleus and contract as the cell migrates into the wound region (DeBiasio et al., 1988; Hahn et al., 1992; Conrad et al., 1993). The transverse fibers undergo a large contraction early in the process of wound healing. It is predicted that calcium–calmodulin binds to MLCK and any other calmodulin targets in the transverse fibers and regulates the contractile activity, since $[Ca^{2+}]_f$ is elevated in this region and calcium binding to calmodulin is detected by the optical biosensor, MeroCam I (Hahn et al., 1992). To test this prediction we coinjected FITC-CaM and ATR-myosin II into fibroblasts during wound healing and compared calmodulin binding as detected by FAIM with the distribution and contraction of transverse fibers identified with the fluorescent analog of myosin II (Fig. 8). Fig. 8 (*a* and *c*) are fluorescence images of the distribution of ATR-myosin II in a cell at two time points (15-min apart) during the lamellar contraction phase of wound healing. The white arrows indicate regions where myosin II has been incorporated into transverse fibers (Fig. 8 *a*). These fibers contracted at a later time point (Fig. 8 *c*), concentrating the myosin II. In the associated FAIM images, we have marked the region corresponding to the fibers (Fig. 8 *b*), and where the fibers have significantly contracted (Fig. 8 *d*). The pattern of elevated anisotropies in this and other regions of the cells reflects the general organization and rearrangement of the myosin II in transverse fibers. In these cells the nucleus exhibits about a 20% higher anisotropy than the surrounding cytoplasm, although there was variability in the nuclear SSFA. These results are consistent with a role of calmodulin binding to targets in transverse fibers during contraction. A major target could be the MLCK that would contribute to the regulation of the myosin II–based contraction responsible for separating and restructuring cells during the initiation of cell locomotion in wound healing (DeBiasio et al., 1988; Conrad et al., 1989; Hahn et al., 1992; Conrad et al., 1993).

Calmodulin Binding Is Elevated in the Tails of Highly Polarized and Migrating Fibroblasts during Wound Healing

The images in Fig. 9 illustrate the general pattern of calmodulin binding and myosin II organization observed in highly polarized, motile cells. Fig. 9 (*a* and *c*) are ATR-myosin II images of two highly polarized Swiss 3T3 fibroblasts, locomoting from left to right. Both cells are undergoing a tail contraction (left end), and a combination of an extension of the leading lamellum and a contraction of the transverse fibers in the cortex. In the corresponding FAIM images we see a ~20% higher anisotropy in the regions of tail retraction (Fig. 9, *b* and *d*), and some locally high anisotropy values in the leading lamellae, the distribution of which resembles the orientations of the fibers in the ATR-myosin II images. Note that the anisotropy in the nucleus of both cells is once again elevated relative to the cytoplasm. Notice also that the perinuclear region of the cell in Fig. 9 *a* exhibits a substantial diffuse myosin II labeling, while the FITC-CaM binding in the FAIM image appears to be low in the perinuclear region. This is the pattern most often observed in motile cells.

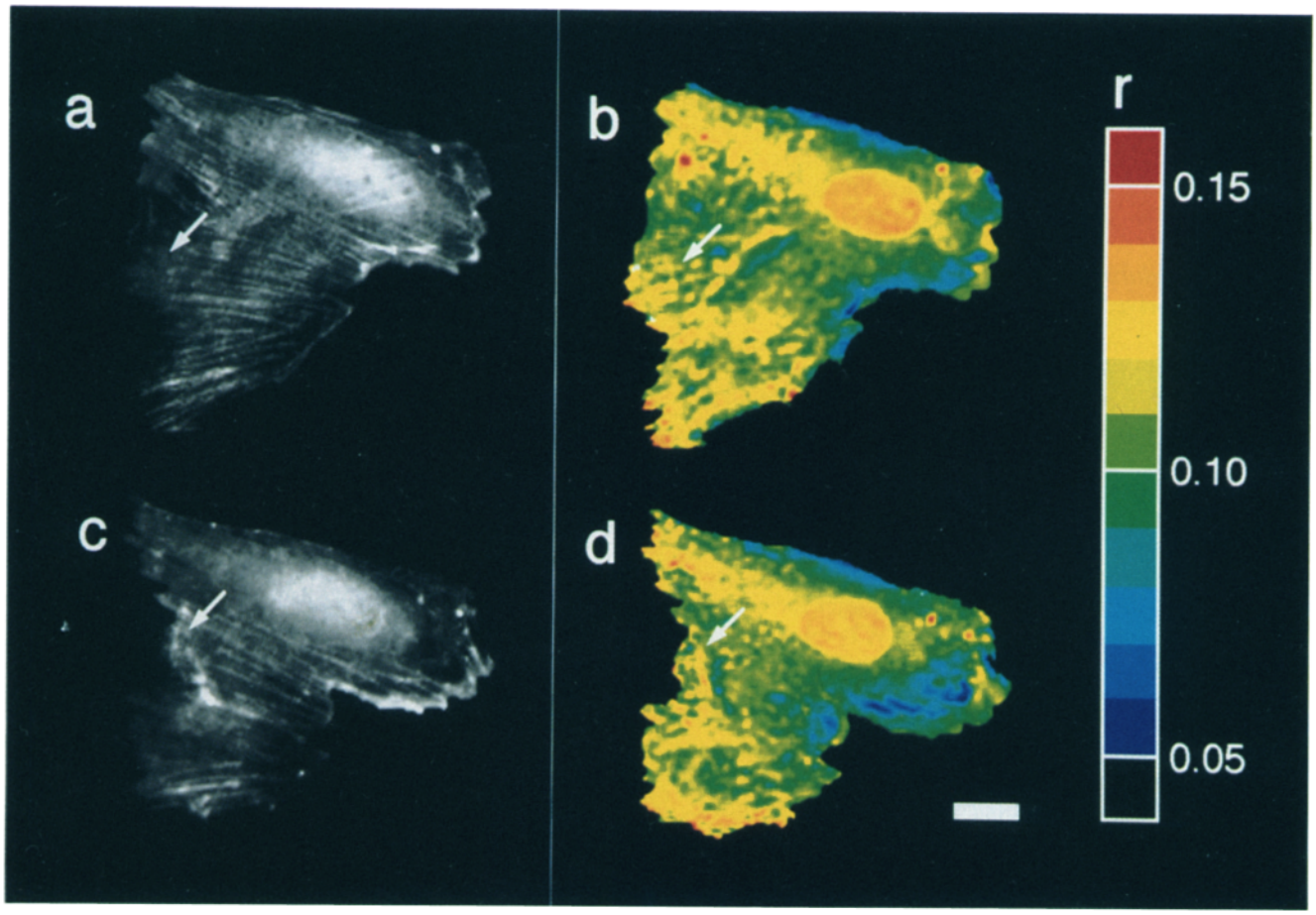

Figure 8.

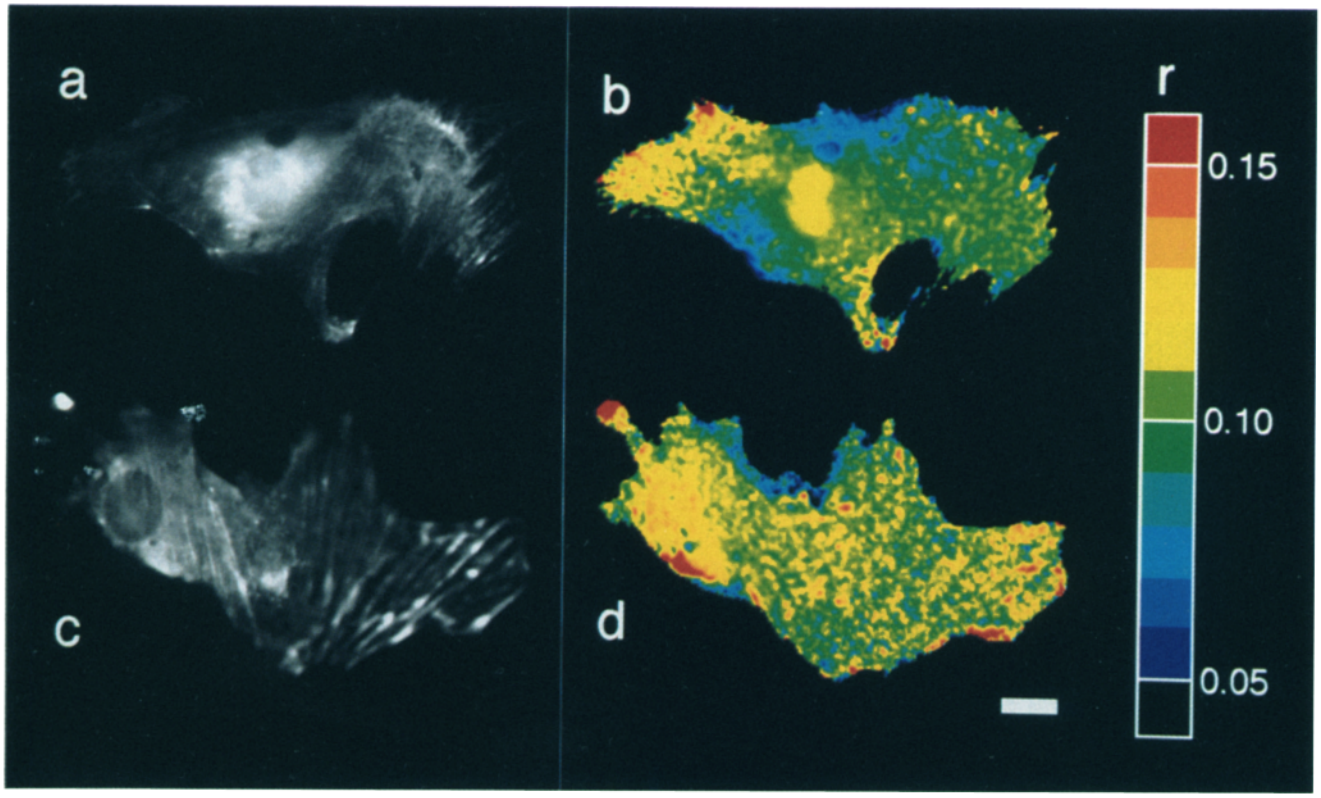

Figure 9.

Discussion

Use of Immunofluorescence, Fluorescent Analogs, and Ratio Imaging

The use of immunofluorescence to map the distribution of calmodulin in a variety of cells at different stages of the cell cycle have resulted in inconsistent interpretations of the localization of calmodulin (Luby-Phelps et al., 1985; Welsh et al., 1978; Willingham et al., 1983; Zavortink et al., 1983). This is not surprising since calmodulin is a relatively small protein and as we have shown, is freely mobile at low $[Ca^{2+}]_f$. Consequently, retention of calmodulin during fixation protocols could be extremely variable and dependent on the specific protocol employed and the state of cellular activation (Melan and Sluder, 1992). Therefore, extreme caution is required to quantitatively interpret fluorescence localization data on a molecule such as calmodulin in the absence of a reference volume indicator (Wang et al., 1982; Luby-Phelps et al., 1985).

Fluorescent analogs can be used to investigate cellular dynamics in living cells, by monitoring changes in the distributions and activities of cellular components (Taylor and Wang, 1978; Wang et al., 1982; Taylor et al., 1984; and Wang, 1989). Ratio imaging has proven to be an important tool for normalizing imaging data for path length, accessible volume, relative concentration of labeled molecules used as environmental indicators, fluorescent analogs, and protein-based optical biosensors (Tanasugarn et al., 1984; Wang et al., 1982; Bright et al., 1989*a*; DeBiasio et al., 1988; Hahn et al., 1992; and this study). The use of fluorescent analogs and the related photo-activated fluorescent analogs (Theriot and Mitchison, 1991), especially in combination with quantitative microscopic methods, should yield important chemical and molecular information in time and space (Taylor et al., 1992).

Our ratio images of FITC-CaM indicate that calmodulin is uniformly distributed in cells at low $[Ca^{2+}]_f$ and remains uniformly distributed during serum-induced calcium transients. However, calmodulin is shown to bind to targets during this same time period. The response of calmodulin to a calcium signal appears to involve local changes in the bound versus free ratio of calmodulin without a dramatic redistribution within the cell. Future studies will explore the interaction of calmodulin with specific target proteins and determine whether any other conditions result in the concentration of calmodulin in any cellular domains.

Steady State FAIM of Calmodulin: Comparison with Previous Fluorescence Methods

This study represents the first application of steady state FAIM to the measurement of protein interactions and macromolecular mobility in living cells. Previous studies of calmodulin mobility in living cells by FRAP were limited to low spatial resolution spot measurements which showed both intracellular and cell to cell variations in the mobility (Luby-Phelps et al., 1985; Stemple et al., 1988) demonstrating that calmodulin exhibited localized interactions. The low spatial resolution of FRAP, and the dependence of the translational mobility on long-range cytoplasmic organization (Luby-Phelps et al., 1987) complicated the interpretation and suggested the need for a method to map mobility in two dimensions. FRAP measurements show that the translational mobilities of nearly all microinjected proteins are reduced substantially from that in simple aqueous solution due to interactions with the cytoplasmic matrix proteins (Luby-Phelps et al., 1987).

The ratio imaging approach to fluorescence polarization measurements, originally proposed by Tanasugarn et al. (1984) has previously been used to investigate the mobility of free dye molecules in vitro and in vivo (Dix and Verkman, 1990; Fushimi and Verkman, 1991; Keating and Wensel, 1991). Measurement of the rotational mobility of dye molecules in cytoplasm indicates that the viscosity of the aqueous phase of cytoplasm is only slightly higher than that of water. The uniform and low values of the anisotropy measured for FITC-CaM and FITC-dextran in this work indicates that the rotational mobility of proteins and macromolecules of up to 16,790 M_r in cytoplasm is not strongly effected by the presence of the cytoplasmic matrix. Instead, macromolecules in this size range tumble about the same as they would in water, and changes in the rotational mobility result from binding interactions. We believe FAIM to be a powerful and simple mode of light microscopy for studying macromolecular interactions in living cells.

Calcium Signaling, the Calmodulin Response, and Contraction of Stress Fibers in Serum-stimulated Cells

The serum-deprived fibroblast has become a valuable model cell for investigating the mechanism and regulation of the formation, transport and contraction of stress fibers (Kolega and Taylor, 1991). The formation, transport, and disassembly of stress fibers occurs as a constitutive process in serum-

Figure 8. Comparison of the distribution of FITC-calmodulin fluorescence anisotropy with the distribution of ATR-Myosin II in transverse fibers during wound healing. (*a* and *c*) Fluorescence images of ATR-Myosin II in a migrating cell during the lamellar contraction phase of wound healing, at two time points 15-min apart. (*b* and *d*) Corresponding FAIM images of FITC-calmodulin. The cells are migrating from the top toward the bottom of the figure, into the wound region. The white arrow indicates a region in which transverse fibers contract between acquisition times. The color scale bar indicates the anisotropy values from 0.04 (*black*) to 0.16 (*red*). Bar, 10 μm.

Figure 9. The distribution of calmodulin binding in highly polarized, migrating cells. Cells were prepared as described in Fig. 8. (*a* and *c*) Fluorescence images of ATR-myosin II in two typical cells migrating from left to right into the wound region. (*b* and *d*) Corresponding FAIM images of the same two cells. Both cells exhibit higher anisotropy in the tail region (*left*), and locally high anisotropies in regions of the leading lamellum containing transverse fibers. The pattern of elevated anisotropy in the leading lamellae is similar to the orientation of the fibers in the same region. The color scale bar indicates the anisotropy values from 0.04 (*black*) to 0.16 (*red*). Bar, 10 μm.

deprived cells (Giuliano and Taylor, 1990). The contraction of stress fibers can be initiated by the addition of complete serum, a purified growth factor, or other pharmacological agents (Giuliano and Taylor, 1990; Giuliano et al., 1992). The stress fibers in stimulated cells contract and disassemble over a 1-h time period, while the elevation of free calcium and calcium binding to calmodulin, upon stimulation, lasts only a few minutes (Hahn et al., 1992). We hypothesize that the serum-deprived fibroblast system reflects general principles of the formation, transport, and contraction of myosin II–based contractile systems in nonmuscle cells including the cleavage furrow (Pollard et al., 1990) and the cell cortex during locomotion (DeBiasio et al., 1988).

The serum-deprived fibroblast exhibits a low free calcium ion concentration (McNeil et al., 1985; McNeil and Taylor, 1987; Byron and Villereal, 1989; Tucker and Fay, 1990; Hahn et al., 1992). Biochemical assays in vitro have demonstrated that calmodulin is free in solution at low free calcium ion concentrations. Therefore, if calmodulin functions the same way in vivo, then the fluorescent analog of calmodulin would be predicted to have a low fluorescence anisotropy value in the serum-deprived state. Our results are consistent with this prediction and demonstrate that a large fraction of calmodulin is part of the soluble phase of cytoplasm (Luby-Phelps et al., 1987; Pagliaro and Taylor, 1988) under condition of low free calcium ion concentration. The uniformly low fluorescence anisotropy suggests that the calmodulin had free rotational mobility throughout the cell, and therefore was not bound to its target molecules. This suggests that the constitutive formation, transport, and disassembly of stress fibers that has been observed in serum-starved cells does not require extensive calmodulin binding to cellular targets. If myosin II motor activity is required for this process it must involve some mechanism other than calcium–calmodulin activated MLCK phosphorylation of the LC_{20} (Giuliano and Taylor, 1990). Since calmodulin is a high affinity subunit of some enzymes, either calmodulin dissociates from the enzymes in serum-deprived cells, the fluorescent analogs did not exchange with this subpopulation of calmodulin-binding proteins or these proteins are present at very low concentrations in serum-deprived cells. The extent of exchange of fluorescent analogs of calmodulin with a variety of potential target enzymes is currently under investigation.

Stimulation of serum-deprived fibroblasts with complete serum induces only a transient rise in free calcium, yet the myosin II–based contraction of stress fibers continues for an hour or more. It has been shown that the binding of calcium to calmodulin reflects the same time course as the calcium transient (Hahn et al., 1992). In contrast, it has been shown by previous SSFA solution biochemistry, that autophosphorylation of the multifunctional calcium–calmodulin-dependent protein kinase traps calcium–calmodulin, increasing the dissociation time 100–1,000-fold (Meyer et al., 1991). The present results demonstrate that calcium signaling in serum-stimulated cells results in the binding of calmodulin to target proteins and that the dissociation of calmodulin occurs with kinetics similar to the decrease in $[Ca^{2+}]_f$. Some signal must continue during the contraction, since calmodulin is only transiently activated. It will be important to determine whether MLCK remains activated by some other mechanism, the phosphatase is inactivated, or there is another force generating regulatory mechanism for myosin II that does not involve calmodulin binding. Recently, it has been shown that an increase in the phosphorylation level of the LC_{20} occurs within seconds of serum stimulation and remains elevated during the ~1 h time period of a contraction (Giuliano et al., 1992). It will also be important to determine how this occurs without continued binding of calmodulin to targets such as MLCK.

The spatial variation in the anisotropy during serum-stimulation could occur as a result of spatial variations in the localization of binding sites for calmodulin, propagation of a calcium wave or differences in the off rate of calcium release from calmodulin once the calcium concentration drops below the K_d (Meyer et al., 1991). Preliminary results with a fluorescent analog of MLCK have indicated that MLCK is relatively uniformly distributed in serum-deprived cells, but the distribution has not been mapped as a function of time following stimulation (Cornwall, T. L., K. A. Giuliano, and D. L. Taylor, unpublished observation). Immunofluorescence mapping of MLCK has indicated that it shows some localization along stress fibers (de Lanerolle et al., 1981), although the question remains as to whether this is total MLCK or a "bound" fraction as discussed above for calmodulin. Although the maximum measured $[Ca^{2+}]_f$ during a transient is $<10^{-6}$ M (McNeil et al., 1985; McNeil and Taylor, 1987; Byron and Villereal, 1989; Tucker and Fay, 1990), measurements of calcium–calmodulin interactions with target proteins are only half maximal at $\sim 10^{-6}$ M (Cohen and Klee, 1988). Our anisotropy results however indicate that at least in some regions of the cell nearly all of the microinjected calmodulin is bound during a calcium transient. Because calmodulin is multifunctional, calcium binding triggers interactions with many calmodulin targets. Higher local concentrations of calmodulin targets could explain this enhanced binding at submicromolar $[Ca^{2+}]_f$, and could result in significant interactions even at lower levels of $[Ca^{2+}]_f$, $\sim 10^{-7}$ M (see below). One future goal is to co-map the distribution of several calmodulin binding proteins and correlate the local concentration with calmodulin binding using multiple parameter fluorescence imaging (DeBiasio et al., 1987; Waggoner et al., 1989) and steady state FAIM.

Patterns of Elevated Free Calcium, Calcium Binding to Calmodulin, and Calmodulin Binding to Target Proteins

Fibroblasts undergoing the wound healing response exhibit a lamellar contractile phase when the transverse fibers in the leading lamellae contract, causing the cells to become narrow and to pull away from neighboring cells (DeBiasio et al., 1988; Conrad et al., 1989; Hahn et al., 1992; Conrad et al., 1993). This myosin II–based contraction was predicted to exhibit increases in calmodulin binding in the domains containing the contracting transverse fibers. The results presented here demonstrate that regions containing contracting transverse fibers also show local regions of increased calmodulin binding as predicted. It has been previously shown that these same regions exhibit elevated free calcium and calcium binding to calmodulin (Hahn et al., 1992). Therefore, the contraction of transverse fibers involves the local elevation of free calcium, calcium binding to calmodulin, and the binding of calmodulin to targets within the region of transverse fibers.

As the cell extends during locomotion, there is a retraction of the tail, believed to involve a myosin II–based contraction. Measurements of free calcium, and calcium binding to calmodulin suggest that there is a gradient of calcium in these polarized migrating cells, that is highest in the rear (Hahn et al., 1992). Our data show that calmodulin binding is higher in the contracting tail as well. A cortical contraction of myosin II-actin that is also transporting from the site of assembly at the leading edge to the perinuclear region could be a component of the mechanism of cell movement that maintains cell shape, optimizes cell polarity, and aids in the delivery of cytoskeletal subunits to the leading edge (Hahn et al., 1992; Conrad et al., 1993). The site of cytoskeletal disassembly could be the perinuclear region where myosin II–based contraction could complete a self-destruct force-generating cycle (Kolega et al., 1991).

Is There Calcium-Calmodulin Targeting in the Cell?

Because calmodulin has many binding sites (targets) in the cell it is not clear whether calcium-based signaling alone activates the full range of calcium–calmodulin regulated processes, or whether there are other regulation schemes in the cell which allow targeting the calmodulin response to particular subsets of the calcium–calmodulin binding sites or particular regions of the cell. There is some evidence that the calcium dependence of the interaction of calmodulin with target proteins is dependent on the concentration of calmodulin (Huang et al., 1981). The presence of a high local concentration of a calmodulin target and sufficient calcium to induce some interactions could result in an increased local concentration of calmodulin and therefore local activation of one calmodulin target relative to another. This positive feedback could provide a mechanism for selective activation of calmodulin targets, such as MLCK, at submicromolar $[Ca^{2+}]_f$, in regions where MLCK has been concentrated by its interaction with myosin II. We are currently developing a method to quantify ratio imaging in terms of analog concentration in order to investigate the possible role of increased local concentrations in calmodulin function. Other mechanisms of targeting a signal to a particular response, such as the trapping of calmodulin by the autophosphorylation of the multifunctional calmodulin kinase II (Meyer et al., 1991), also need to be investigated.

Future Directions

While this study demonstrates the use of FAIM in deciphering the role of calmodulin in regulating cellular processes, real time FAIM measurements in conjunction with other modes of light microscopy, including $[Ca^{2+}]_f$ ion measurements and mapping a variety of calmodulin targets, will allow a more detailed characterization of the sequence of signaling and effector steps. Presently, an instrument is being developed that will allow simultaneous acquisition of the parallel and perpendicular images (Taylor and Zeh, 1976; Kinosita et al., 1991), as well as simultaneous pairs of ratio images, to improve temporal resolution, while reducing the total illumination, so that longer sequences of images can be acquired. Furthermore, FAIM can be applied to laser confocal scanning microscopes with a minimum of complications. Time resolved fluorescence microscopy can also be used to study molecular interactions and other parameters which influence the lifetime of the excited state (Fushimi and Verkman, 1991; Keating and Wensel, 1991; Lakowicz et al., 1991). The advantages of steady state FAIM, compared with time resolved methods are the minimal requirement for additional instrumentation, the ability to correlate spectroscopic information with high-resolution morphological data and the simplicity of the measurements. However, time-resolved fluorescence microscopy has the advantage of distinguishing multiple populations of fluorophores in different environments and being independent of fluorescence intensity. Both steady state FAIM and time resolved methods should yield exciting information about cellular chemistry and molecular interactions in vivo.

Appendix

Principle of Steady State Fluorescence Anisotropy Measurements

The steady state fluorescence anisotropy (r) is defined as:

$$r = (I_{par} - G^*I_{prp})/(I_{par} + 2G^*I_{prp}), \quad \text{(A1)}$$

where I_{par} and I_{prp} represent the image (intensity) with the excitation and emission polarizers oriented parallel and perpendicular, respectively, and G is a factor which corrects for differential polarization sensitivity of the detection system (Lakowicz, 1983). A simple rearrangement of this equation shows that the fluorescence anisotropy depends on the ratio between I_{par} and I_{prp}, and therefore corrects any shading effects in the imaging system (see Image Processing). The denominator of Eq. (A1) represents the total fluorescence emission, and therefore normalizes for differences in intensity due to concentration and path length. When measuring intensities at high numerical aperture, this normalization is not strictly correct, because the polarization at the fringe of the field is rotated (Axelrod, 1979, 1989). However, measurements on solutions over a wide range of concentrations show that the effect was not significant (data not shown). Furthermore, this effect only tends to reduce the anisotropy values at higher brightness, because there is an extra contribution to the intensity of both the parallel and perpendicular orientations that cancels in the numerator while adding to the denominator.

The SSFA depends on the relative magnitudes of the fluorescence lifetime (τ_f) and the rotational correlation time (ϕ) as described by the Perrin equation (Lakowicz, 1983):

$$r = r_o\,(\phi/(\phi + \tau_f)), \quad \text{(A2)}$$

where r_o is the anisotropy in the absence of rotation. From Eq. (A2) it is apparent that if $\tau_f << \phi$, r approaches r_o and becomes insensitive to changes in ϕ, and if $\tau_f >> \phi$, r will be small and therefore difficult to measure. Therefore, a fluorophore must be chosen such that $\tau_f \sim \phi$. The rotational diffusion coefficient ($D_R = (6\phi)^{-1}$) is related to the hydrodynamic radius (R_H) and the viscosity (η) by the Stokes-Einstein equation:

$$D_R = (kT)/(8\pi\eta R_H^3), \quad \text{(A3)}$$

where k is the Boltzman constant and T is the temperature in Kelvin. Thus, the SSFA depends on τ_f, r_o, T, η, and R_H^3. In this study we take advantage of the size dependence to detect calmodulin binding in cells.

Image Processing

Images were stored as arrays of 16-bit integers, background subtracted, registered, and corrected for bleaching before anisotropy calculations. The background was taken from each image in a region of the image with no cells. The shift of the perpendicular image relative to the parallel image, probably due to wedge in the mounted polarizer, was determined from images of fluorescent beads to be slightly more than 1 pixel, was constant from day to day, and was corrected by shifting the perpendicular images using an appropriate convolution kernel. The bleaching correction factor was determined for each acquisition series from the ratio between the first parallel image ($I_{\parallel 1}$) and the second parallel image ($I_{\parallel 2}$) and was $\leqslant 3\%$ per image. Since the integration time, T, is constant, the excitation intensity, E, is con-

stant, and assuming the bleaching rate is constant, the fraction remaining after bleaching for one acquisition cycle will be constant (f_b). The intensities will be different however, for the two different positions of the emission polarization analyzer, so two images acquired with the same analyzer orientation were used to determine the bleaching correction factor. Since the parallel and perpendicular images are acquired alternately, the intensity in the second parallel image, $I_{\parallel 2}$, will be reduced by two acquisition cycles. The bleaching corrected perpendicular image ($I'_{\perp 1}$) can be determined from the preceding and following parallel images as follows:

$$\frac{I_{\parallel 2}}{I_{\parallel 1}} = f_b^2 \; so \; I'_{\perp 1} = \left[\frac{I_{\parallel 1}}{I_{\parallel 2}}\right]^{1/2} I_{\perp 1}. \tag{A4}$$

The bleaching correction factor (per integration time) is thus the square root of the ratio between the first parallel image and the second parallel image. Anisotropy values were checked for bleaching effects by calculating the anisotropy from image pairs both in the same order as acquired and in the reverse order. For example, after correction for bleaching the average value of $r(I_{\parallel 1}, I_{\perp 1})$ was approximately equal to the average value of $r(I_{\parallel 2}$ $I_{\perp 1})$, where $I_{\parallel 1}$ was acquired immediately before $I_{\perp 1}$ and $I_{\parallel 2}$ was acquired immediately after $I_{\perp 1}$.

Images for calculating the G correction factor were acquired from a 1 μM sodium fluorescein solution in 50 mM Tris, pH 8.5, loaded into a 50-μm path length flat capillary (Vitro Dynamics, Rockaway, NJ). Parallel and perpendicular background images were acquired from a similar capillary loaded with water. The anisotropy of this solution as measured on the fluorometer was 0.011 and, after background subtraction, the G factor was calculated as described by Dix and Verkman (1990). The G factor, uniform across the field, had a value of 0.814 and was constant from day to day. The anisotropy (r) was calculated in floating point as $r = [(I_\parallel/I_\perp) - G]/[(I_\parallel/I_\perp) + 2G]$ using TCL-Image (Biological Detection Systems, Pittsburgh, PA). The floating point FAIM images were multiplied by 32,768 and stored as arrays of 16-bit integers. Since the maximum theoretical SSFA value in this case is 0.4, this scaling factor ensures that the output integer values have sufficient dynamic range to preserve detail. Images were displayed and pseudo-colored in NIH Image version 1.44.

Choosing a Probe for Fluorescence Anisotropy Measurements

The SSFA depends on the ratio between the fluorescence lifetime (τ) and the rotational correlation time (ϕ), the viscosity, and the hydrodynamic radius of the molecule (see Eqs. A2 and A3). The fluorescence lifetime is the average time that a fluorescent molecule remains in the excited state and the rotational correlation time is the time it takes for a population of molecules with anisotropic orientations to become isotropic. The dependence on τ_f/ϕ necessitates using a fluorophore with a lifetime of the same order as the expected rotational correlation time, 7–10 ns for calmodulin (Lambooy et al., 1982). Because the fluorescence lifetime is inversely related to both the molar extinction coefficient and excitation wavelength (Strickler and Berg, 1962), fluorescent dyes with lifetimes this long are not very bright and have short excitation wavelengths. As an example, Bimane-CaM has τ_f=9.5 ns, but a relatively small extinction coefficient of 5,300 and a 380 nm maximal excitation wavelength. At the other end of the spectrum, TRITC-CaM has an extinction coefficient of 85,000 and the excitation wavelength is 554 nm, but τ_f is only 2 ns (Table I), making it an excellent choice for imaging but limiting its use as a probe of macromolecular rotational mobility to only small molecules (~2–8 kDa).

We would like to give special thanks to Robbin DeBiasio for performing the FITC-CaM/rhodamine-dextran control experiments. We would also like to thank Ken Giuliano, John Kolega, Fred Lanni, and other members of the Center for Light Microscope Imaging and Biotechnology, for their helpful discussions and comments on this work.

This research was supported by National Science Foundation Science and Technology Center Grant DIR-8920118, National Institutes of Health Grant AR 32461-11, and Council for Tobacco Research–USA Award 2044A.

Received for publication 5 October 1992 and in revised form 16 March 1993.

References

Axelrod, D. 1979. Carbocyanine dye orientation in red cell membrane studied by microscopic fluorescence polarization. *Biophys. J.* 26:557–574.

Axelrod, D. 1989. Fluorescence polarization microscopy. *In* Fluorescence Microscopy of Living Cells in Culture Part B. Quantitative Fluorescence Microscopy–Imaging and Spectroscopy. D. L. Taylor and Y. Wang, editors. Academic Press, Inc., San Diego, CA. 333–352.

Bright, G. R., G. W. Fisher, J. Rogowska, and D. L. Taylor. 1987. Fluorescence ratio imaging microscopy: temporal and spatial measurements of cytoplasmic pH. *J. Cell Biol.* 104:1019–1033.

Bright, G. R., G. W. Fisher, J. Rogowska, and D. L. Taylor. 1989*a*. Fluorescence ratio imaging microscopy. *In* Fluorescence Microscopy of Living Cells in Culture Part B. Quantitative Fluorescence Microscopy–Imaging and Spectroscopy. D. L. Taylor and Y. Wang, editors. Academic Press, Inc., San Diego, CA. 157–190.

Bright, G. R., J. E. Whitaker, R. P. Haugland, and D. L. Taylor. 1989*b*. Heterogeneity of the changes in cytoplasmic pH upon serum stimulation of quiescent fibroblasts. *J. Cell. Physiology* 141:410–419.

Byron, K. L., and M. L. Villereal. 1989. Mitogen-induced [Ca^{2+}]i changes in individual human fibroblasts. Image analysis reveals asynchronous responses which are characteristic for different mitogens. *J. Biol. Chem.* 264:18234–18239.

Chen, R. F., and C. H. Scott. 1985. Atlas of fluorescence spectra and lifetimes of dyes attached to proteins. *Anal. Lett.* 18(A4):393–421.

Cohen, P., and C. B. Klee. 1988. Criteria required to demonstrate calmodulin-dependent effects in vivo. *In* Calmodulin. P. Cohen and C. B. Klee, editors. Elsevier, Amsterdam, The Netherlands. 357–363.

Conrad, P. A., M. A. Nederlof, I. M. Herman, and D. L. Taylor. 1989. Correlated distribution of actin, myosin, and microtubules at the leading edge of migrating Swiss 3T3 fibroblasts. *Cell Motil. Cytoskeleton.* 14:527–543.

Conrad, P. A., K. A. Giuliano, G. W. Fisher, K. Collins, P. Matsudaira, and D. L. Taylor. 1993. Relative distribution of actin, myosin I and myosin II during the wound healing response of fibroblasts. *J. Cell Biol.* 120:1381–1391.

DeBiasio, R. L., L. L. Wang, G. W. Fisher, and D. L. Taylor. 1988. The dynamic distribution of fluorescent analogues of actin and myosin in protrusions at the leading edge of migrating Swiss 3T3 fibroblasts. *J. Cell Biol.* 107:2631–2645.

de Lanerolle, P., R. S. Adelstein, J. R. Feramisco, and K. Burridge. 1981. Characterization of antibodies to smooth muscle myosin kinase and their use in localizing myosin kinase in nonmuscle cells. *Proc. Natl. Acad. Sci. USA.* 78:4738–4742.

Dix, J. A., and A. S. Verkman. 1990. Mapping of fluorescence anisotropy in living cells by ratio imaging: application to cytoplasmic viscosity. *Biophys. J.* 57:231–240.

Fisher, G. W., P. A. Conrad, R. L. DeBiasio, and D. L. Taylor. 1988. Centripetal transport of cytoplasm, actin, and the cell surface in lamellipodia of fibroblasts. *Cell Motil. Cytoskeleton.* 11:235–247.

Fushimi, K., and A. S. Verkman. 1991. Low viscosity in the aqueous domain of cell cytoplasm measured by picosecond polarization microfluorimetry. *J. Cell Biol.* 112:719–725.

Giuliano, K. A., and D. L. Taylor. 1990. Formation, transport, contraction, and disassembly of stress fibers in fibroblasts. *Cell Motil. Cytoskeleton.* 16:14–21.

Giuliano, K. A., J. Kolega, R. L. DeBiasio, and D. L. Taylor. 1992. Myosin II phosphorylation and the dynamics of stress fibers in serum-deprived and stimulated fibroblasts. *Mol. Biol. Chem.* 3:1037–1048.

Hahn, K. M., A. S. Waggoner, and D. L. Taylor. 1990. A calcium-sensitive fluorescent analog of calmodulin based on a novel calmodulin-binding fluorophore. *J. Biol. Chem.* 265:20335–20345.

Hahn, K. M., R. DeBiasio, and D. L. Taylor. 1992. Patterns of elevated free calcium and calmodulin activation in living cells. *Nature (Lond.).* 359: 736–738.

Huang, C. Y., V. Chau, P. B. Chock, J. H. Wang, and R. K. Sharma. 1981. Mechanism of activation of cyclic nucleotide phosphodiesterase: requirement of the binding of four Ca^{2+} to calmodulin for activation. *Proc. Natl. Acad. Sci. USA.* 78:871–874.

Keating, S. M., and T. G. Wensel. 1991. Nanosecond fluorescence microscopy: emission kinetics of Fura-2 in single cells. *Biophys. J.* 59:186–202.

Kinosita Jr., K., H. Itoh, S. Ishiwata, K. Hirano, T. Nishikaza, and T. Hayakawa. 1991. Dual view microscopy with a single camera: real-time imaging of molecular orientations and calcium. *J. Cell Biol.* 115:67–73.

Kolega, J., and D. L. Taylor. 1991. Regulation of actin and myosin II dynamics in living cells. *Curr. Top. Membr.* 38:187–206.

Kolega, J., L. W. Janson, and D. L. Taylor. 1991. The role of solation-contraction coupling in regulating stress fiber dynamics in nonmuscle cells. *J. Cell Biol.* 114:993–1003.

Kosower, N. S., and E. M. Kosower. 1987. Thiol labeling with bromobimanes. *Methods Enzymol.* 143:76–84.

Lakowicz, J. R. 1983. Fluorescence polarization. *In* Principles of Fluorescence Spectroscopy. Plenum Press, New York. 112–150.

Lakowicz, J. R., and K. W. Berndt. 1991. Lifetime-selective fluorescence imaging using an RF phase-sensitive camera. *Rev. Sci. Inst.* 62:1727–1734.

Lambooy, P. K., R. F. Steiner, and H. Sternberg. 1982. Molecular dynamics of calmodulin as monitored by fluorescence anisotropy. *Arch. Biochem. Biophys.* 217:517–528.

Luby-Phelps, K., F. Lanni, and D. L. Taylor. 1985. Behavior of a fluorescent

analogue of calmodulin in living 3T3 cells. *J. Cell Biol.* 101:1245–1256.
Luby-Phelps, K., P. E. Castle, D. L. Taylor, and F. Lanni. 1987. Hindered diffusion of inert tracer particles in the cytoplasm and of mouse 3T3 cells. *Proc. Natl. Acad. Sci. USA.* 84:4910–4913.
Luby-Phelps, K., F. Lanni, and D. L. Taylor. 1988. The submicroscopic properties of cytoplasm as a determinant of cellular function. *Ann. Rev. Biophys. Chem.* 17:369–396.
McNeil, P. L., and D. L. Taylor. 1987. Early cytoplasmic signals and cytoskeletal responses initiated by growth factors in cultured cells. *Cell Membr.* 3:365–405.
McNeil, P. L., M. P. McKenna, and D. L. Taylor. 1985. A transient rise in cytosolic calcium follows stimulation of quiescent cells with growth factors and is inhibitable with phorbol myristate acetate. *J. Cell Biol.* 101:372–379.
Melan, M. A., and G. Sluder. 1992. Redistribution and differential extraction of soluble proteins in permeabilized cultured cells. Implications for immunofluorescence microscopy. *J. Cell Sci.* 101:731–743.
Meyer, T., P. I. Hanson, L. Stryer, and H. Schulman. 1991. Calmodulin trapping by calcium-calmodulin-dependent protein kinase. *Science (Wash. DC).* 256:1199–1202.
Mills, J., M. Walsh, K. Nemcek, and J. Johnson. 1988. Biologically active fluorescent derivatives of spinach calmodulin that report calmodulin target protein binding. *Biochemistry.* 27:991–996.
Pagliaro, L., and D. L. Taylor. 1988. Aldolase exists in both the fluid and solid phases of cytoplasm. *J. Cell Biol.* 107:981–991.
Robertson, S., and J. D. Potter. 1984. The regulation of free Ca^{++} ion concentration by metal chelators. *Methods Pharmacol.* 5:63–74.
Schiefer, S. 1986. Calmodulin. *Methods Enzym. Analy.* IX:317–331.
Sellers, J. R., and R. S. Adelstein. 1987. Regulation of contractile activity. *Enzymes.* 18:381–418.
Simon, J. R., A. Gough, E. Urbanik, F. Wang, F. Lanni, B. R. Ware, and D. L. Taylor. 1988. Analysis of rhodamine and fluorescein-labeled F-actin diffusion in vitro by fluorescence photobleaching recovery. *Biophys. J.* 54:801–815.
Stemple, D. L., S. C. Sweet, M. J. Welsh, and J. R. McIntosh. 1988. Dynamics of a fluorescent calmodulin analog in the mammalian mitotic spindle at metaphase. *Cell Motil. Cytoskeleton.* 9:231–242.
Strickler, S. J., and R. A. Berg. 1962. Relationship between absorption intensity and fluorescence lifetime of molecules. *J. Chem. Physiol.* 37:814–822.
Tanasugarn, L., P. McNeil, G. Reynolds, and D. L. Taylor. 1984. Microspectrofluorometry by digital image processing: measurement of cytoplasmic pH. *J. Cell Biol.* 98:717–724.
Taylor, D. L., and R. Zeh. 1977. Methods for the measurement of polarization optical properties: I. Birefringence. *J. Microscopy.* 108:251–259.
Taylor, D. L., and Y. L. Wang. 1978. Molecular cytochemistry: incorporation of fluorescently labeled actin into living cells. *Proc. Natl. Acad. Sci. USA.* 75:857–861.
Taylor, D. L., and Y. L. Wang. 1980. Fluorescently labeled molecules as probes of the structure and function of living cells. *Nature (Lond.).* 284:405–410.
Taylor, D. L., P. A. Amato, K. Luby-Phelps, and P. L. McNeil. 1984. Fluorescent analog cytochemistry. *Trends Biochem. Sci.* 9:88–91.
Taylor, D. L., P. A. Amato, P. L. McNeil, K. Luby-Phelps, and L. Tanasugarn. 1986. Spatial and temporal dynamics of specific molecules and ions in living cells. *In* Applications of Fluorescence in the Biomedical Sciences. D. L. Taylor, A. S. Waggoner, R. F. Murphy, F. Lanni, and R. R. Birge, editors. Alan R. Liss, Inc., New York. 347–376.
Taylor, D. L., M. Nederlof, F. Lanni, and A. S. Waggoner. 1992. The new vision of light microscopy. *Am. Sci.* 80:322–335.
Theriot, J. A., and T. J. Mitchison. 1991. Actin microfilament dynamics in locomoting cells. *Nature (Lond.).* 352:126–131.
Tucker, R. W., and F. S. Fay. 1990. Distribution of intracellular free calcium in quiescent BALB/c 3T3 cells stimulated by platelet-derived growth factor. *Eur. J. Cell Biol.* 51:120–127.
Waggoner, A. S. 1986. Fluorescent probes for analysis of cell structure, function, and health by flow and imaging cytometry. *In* Applications of Fluorescence in the Biomedical Sciences. D. L. Taylor, A. S. Waggoner, R. F. Murphy, F. Lanni, and R. R. Birge, editors. Alan R. Liss, Inc., New York. 3–28.
Waggoner, A. S. 1990. Fluorescent probes for cytometry. *In* Flow Cytometry and Sorting. M. R. Melamed, T. Lindmo, and M. L. Mendelsohn, editors. Wiley-Liss, Inc., New York. 209–225.
Waggoner, A., R. DeBiasio, P. Conrad, G. R. Bright, L. Ernst, K. Ryan, M. Nederlof, and D. Taylor. 1989. Multiple spectral parameter imaging. *In* Fluorescence Microscopy of Living Cells in Culture Part B. Quantitative Fluorescence Microscopy—Imaging and Spectroscopy. D. L. Taylor and Y. Wang, editors. Academic Press, Inc., San Diego, CA. 333–352.
Wang, Y. 1989. Fluorescent Analog Cytochemistry: tracing functional protein components in living cells. *In* Fluorescence Microscopy of Living Cells in Culture Part A. Fluorescent Analogs, Labeling Cells, and Basic Microscopy. Y. Wang and D. L. Taylor, editors. Academic Press, Inc., San Diego, CA. 1–12.
Wang, Y. L., J. M. Heiple, and D. L. Taylor. 1982. Fluorescent analog cytochemistry of contractile proteins. *Methods Cell Biol.* 25(B):1–11.
Welsh, M. J., J. R. Dedman, B. R. Brinkley, and A. R. Means. 1978. Calcium-dependent regulator protein: localization in mitotic apparatus of eukaryotic cells. *Proc. Natl. Acad. Sci. USA.* 75:1867–1871.
Willingham, M. C., C. J. Wehland, C. B. Klee, N. D. Richer, A. V. Rutherford, and I. H. Pastan. 1983. Ultrastructural immunocytochemical localization of calmodulin in cultured cells. *J. Histochem. Cytochem.* 31:445–461.
Zavortink, M., M. J. Welsh, and J. R. McIntosh. 1983. The distribution of calmodulin in living cells. *Exp. Cell Res.* 149:375–385.